Polyhedron 245 (2023) 116659

Contents lists available at ScienceDirect

Polyhedron

journal homepage: www.elsevier.com/locate/poly

Influence of metal on coordination geometry and solution dynamics in complexes of *cis*-ethylene*bis*(diphenylphosphine oxide) and Ln(OTf)$_3$ (Ln = La, Sm, Lu) X-ray crystal structures and NMR titration studies

Georgia G. Sands [a], Grace Ertle [a], Jimmy Mugemana [a], Richard J. Staples [b], John E. Bender [a], Shannon M. Biros [a,*]

[a] Department of Chemistry, Grand Valley State University, 1 Campus Dr., Allendale, MI 49401, United States
[b] Center for Crystallographic Research, Department of Chemistry, Michigan State University, 578 S. Shaw Lane, East Lansing, MI 48824, United States

ARTICLE INFO

Keywords:
Lanthanide coordination chemistry
Crystal structure
Phosphine oxide ligand

ABSTRACT

This paper describes the synthesis and characterization of complexes containing the relatively rigid *bis*phosphine oxide ligand *cis*-ethylene*bis*(diphenylphosphine oxide) with three lanthanide (Ln) triflate salts (Ln = La^{3+}, Sm^{3+}, Lu^{3+}). The complexes were characterized in the solid state by IR and X-Ray crystallography and show bidentate binding of the ligand to each metal center. The complexes were also studied at various Ln-ligand stoichiometries in solutions of $CDCl_3$ using ^1H and ^{31}P NMR. These studies revealed that for the complexes where Ln = La^{3+} and Sm^{3+} ligand exchange is fast on the ^1H and ^{31}P NMR time scales when there are less than four equivalents of ligand in solution but slows when more than four equivalents are present. For the solution studies of complexes with Lu^{3+}, ligand exchange is fast on the ^1H NMR but slow on the ^{31}P NMR time scale for all Lu-ligand stoichiometries.

1. Introduction

Research into *f*-block elements has gained interest due to applications in areas such as luminescent bioprobes [1], electronic spin qubits [2], and energy production [3]. Some specific examples of the diverse applications *f*-elements have found use in include pain treatment in metastatic bone cancer (^{153}Sm) [4], removal of phosphorus from wastewater (La) [5], and photocatalysis (lutetium doped nanoparticles) [6,7]. Since many of these applications involve the complexation of a *f*-block metal with an organic ligand, research into the synthesis and characterization of new lanthanide-ligand complexes could lead to advances in these spheres of research.

The organic ligand investigated in this study is *cis*-ethylene*bis* (diphenylphosphine oxide) (dppeO_2) shown in Scheme 1. Single crystal X-ray diffraction structures of this relatively rigid *bis*phosphine oxide ligand complexed with manganese [8] and tin [9–12] have been published, as well as with the *f*-element thorium [13]. In almost all of these structures this ligand binds to the metal in a bidentate manner in the solid state. Other groups have studied the ability of this ligand to separate lanthanide (Ln) and actinide (An) ions in solution [14–18], with a potential use of this chemistry for the recycling of *f*-elements [19,20] and for the treatment of spent nuclear fuel [21].

We add to the current body of knowledge on the coordination chemistry of *cis*-dppeO_2 with this work, where this ligand was complexed with the three lanthanide triflate (OTf) salts La(OTf)$_3$, Sm(OTf)$_3$, and Lu(OTf)$_3$. This study includes characterization of the resulting complexes in both the solid state (X-ray crystallography, IR, CHN) and in solution (NMR, MS). We chose to prepare complexes where Ln(III) = La, Sm and Lu since complexes containing those three lanthanide metals give NMR spectra that do not suffer from severe line broadening. Our goal at the outset of this work was to probe the effect of Ln^{3+} size on the geometry and stoichiometry of the resultant complexes.

2. Materials and methods

2.1. General considerations

All chemicals (including deuterated solvents) were purchased from

Abbreviations: Ln, lanthanide; dppeO_2, *cis*-ethylene*bis*(diphenylphosphine oxide); LR ESI-MS, low resolution electrospray ionization mass spectrometry; OTf, triflate.

* Corresponding author.
E-mail address: biross@gvsu.edu (S.M. Biros).

https://doi.org/10.1016/j.poly.2023.116659
Received 18 July 2023; Accepted 9 September 2023
Available online 11 September 2023

Sigma-Aldrich or Strem Chemical and used without further purification. NMR spectral data (^{1}H, ^{13}C, ^{31}P) were recorded on a JEOL ECZS 400 NMR Spectrometer. For NMR spectra, chemical shifts are expressed as parts per million (δ) relative to $SiMe_4$ (TMS, $\delta = 0$) for ^{1}H and ^{13}C data, and H_3PO_4 ($\delta = 0$) for ^{31}P data. Both ^{13}C and ^{31}P NMR spectra were obtained as proton-decoupled data. IR spectra were acquired neat on a Jasco 4100 FTIR. Elemental (CHN) analyses were performed by Atlantic Microlab Inc., Norcross, GA; all CHN percentages calculated for lanthanide complexes assume three phosphine oxide ligands + $Ln(OTf)_3$ + residual water/solvents as indicated. Low-resolution mass spectrometry data were acquired on an Advion Expression-L Compact Mass Spectrometer in ESI mode.

2.2. X-ray diffraction data

The structure of $[La(dppeO_2)_2(OTf)_3(H_2O)_2]$ was obtained using a Bruker Apex-II CCD (charge coupled device) based diffractometer equipped with an Oxford Cryostream low-temperature apparatus operating at 173 K. The total number of images was based on results from the program COSMO [22] where redundancy was expected to be 4.0 and completeness of 100% out to 0.83 Å. Cell parameters were retrieved using APEX II software [23] and refined using SAINT on all observed reflections. Data reduction was performed using the SAINT software [24], which corrects for Lorentz polarization. Scaling and absorption corrections were applied using SADABS [25] multi-scan technique, supplied by George Sheldrick. Details regarding the modeling of disorder and the removal of electron density using the BYPASS procedure [26] are included in the supplemental information file.

The remaining structures presented here were obtained using a Rigaku XtaLAB Synergy, Dualflex, HyPix diffractometer. CRI Data were measured using *w* scans using Cu K_a radiation (micro-focus sealed X-ray tube, 50 kV, 1 mA). The total number of runs and images was based on the strategy calculation from the program CrysAlisPro [27]. Cell parameters were retrieved and refined, and data reduction was performed using CrysAlisPro software [27], which corrects for Lorentz polarization. Numerical absorption correction was based on Gaussian integration over a multifaceted crystal model. Empirical absorption correction using spherical harmonics was implemented in SCALE3 ABSPACK scaling algorithm.

2.3. Synthesis

***cis*-dppeO$_2$.** This compound was prepared according to previously published procedures [13,28]. Here, we altered only the recrystallization step by adding a small amount of DMSO to decrease the amount of benzene required to purify the product. A detailed procedure, along with spectroscopic data, can be found in the Supplemental Information file.

Ln(dppeO$_2$)$_3$(OTf)$_3$ complexes, general procedure. *cis*-$dppeO_2$ (50 mg, 0.116 mmol) and the desired $Ln(OTf)_3$ (Ln = La, Sm, Lu; 0.039 mmol) were dissolved in acetonitrile (20 mL) in a 50 mL round bottom flask. The solution was stirred for 30 min at room temperature, and the volatiles were removed under reduced pressure. The resultant white solids were triturated with diethyl ether (3 × 3 mL) to give thick white oils for the La^{3+} and Sm^{3+} complexes, while the Lu^{3+} complex remained a white powder. The diethyl ether was removed via pipette and the remaining volatiles were removed under high vacuum to give the $[Ln(dppeO_2)_3(OTf)_3(Et_2O)]$ complexes as white solids.

[La(dppeO$_2$)$_3$(OTf)$_3$]. This complex was isolated as an off-white powder (62 mg, 82% yield). FT-IR (cm^{-1}): ν 1438 (C═C), 1155 (P═O). ^{1}H NMR (CD_3CN, 400 MHz): δ 7.46 (bm, 12H), 7.32–6.79 (bm, 8H); ^{1}H NMR ($CDCl_3$, 400 MHz): δ 7.50–7.46 (m, 10*H*), 7.34–7.31 (m, 5H), 7.03 (b, 8H); ^{31}P (CD_3CN, 161 MHz): δ 26.49 (s); ^{31}P ($CDCl_3$, 161 MHz): δ 26.03 (s); ^{13}C NMR (CD_3CN, 100 MHz): δ 129.3 (t, J_{CP} = 5 Hz, C_{ortho}), 131.5 (b, C_{meta}), 133.5 (s, C═*C*), 142.1 (d, J_{CP} = 85 Hz, C_{ipso}); ^{13}C NMR ($CDCl_3$, 100 MHz): δ 129.2 (t, J_{CP} = 6 Hz, C_{ortho}), 131.5 (b, C_{meta}), 133.2 (s, C═*C*), 144.2 (d, J_{CP} = 90 Hz, C_{ipso}); ESI-LRMS (1%) *m/z* calcd for $[La(C_{26}H_{23}O_2P_2)_3(CF_3O_3S)_2(CF_3O_2SOH)(CH_3CN)]^{+}$: 1912.1, found 1913.0; CHN analysis for La(**1**)$_3$(OTf)$_3$(Et$_2$O) calculated (found): C 52.48 (52.57), H 3.92 (3.94), N 0.00 (0.00).

[Sm(dppeO$_2$)$_3$(OTf)$_3$]. This complex was isolated as an off-white powder (67 mg, 88% yield). FT-IR (cm^{-1}): ν 1439 (C═C), 1147 (P═O); ^{1}H NMR (CD_3CN, 400 MHz): δ 7.75–7.41 (m, 4H), 7.21 (bm, 8H), 7.11–7.07 (m, 8H); ^{1}H NMR ($CDCl_3$), 400 MHz): δ 7.05 (bm, 8H), 7.31–7.35 (m, 12H), 8.27 (bm, 2H); ^{31}P (CD_3CN, 161 MHz): δ 27.68 (s); ^{31}P ($CDCl_3$, 161 MHz): δ 26.90 (s); ^{13}C NMR (CD_3CN, 100 MHz): δ 129.3 (t, J_{CP} = 6 Hz, C_{ortho}), 131.3 (t, 5 Hz, C_{meta}), 133.6 (s, C═C), 143.8 (d, J_{CP} = 91 Hz, C_{ipso}), 120.8; ^{13}C NMR ($CDCl_3$, 100 MHz): δ 129.2 (t, J_{CP} = 6 Hz, C_{ortho}), 131.1 (t, 5.6 Hz, C_{meta}), 133.3 (s, C═*C*), 144.2 (d, J_{CP} = 90 Hz, C_{ipso}); ESI-LRMS (1%) calcd for $[Sm(C_{26}H_{23}O_2P_2)_4(CF_3O_3S)(CF_3O_2SOH)(H_2O)(C_2H_6O)]^{2+}$: 1128.7, found 1128.8; CHN analysis for Sm(**1**)$_3$(OTf)$_3$(Et$_2$O) calculated (found): C 52.17 (52.53), H 3.91 (3.86), N 0.00 (0.00).

[Lu(dppeO$_2$)$_3$(OTf)$_3$]. This complex was isolated as an off-white powder (74 mg, 96% yield). FT-IR (cm^{-1}): ν 1438 (C═C), 1147 (P═O). ^{1}H NMR (CD_3CN, 400 MHz): δ 7.86 (t, J_{HP} = 36 Hz, 1H), 7.52–7.47 (m, 8H), 7.37–7.33 (m, 5H), 7.09–7.05 (m, 8H); ^{1}H NMR ($CDCl_3$, 400 MHz): δ 7.86 (t, J_{HP} = 34.4, 1H), 7.50 (q, J_{HP} = 8, 8H), 7.35 (t, J_{HP} = 8 Hz, 6H), 7.09–7.05 (m, 8H). ^{31}P (CD_3CN, 161 MHz): δ 28.29 (s), 26.95 (s), 23.53 (s); ^{31}P ($CDCl_3$, 161 MHz): δ 36.69 (s), 32.31 (s), 28.84 (s). ^{13}C NMR ($CDCl_3$, 100 MHz): δ 143.1 (d, J_{CP} = 97 Hz, C_{ipso}) 133.5 (s, C═C), 131.2 (m, C_{meta}), 129.7–129.1 (m, C_{ortho}). ^{13}C NMR (CD_3CN, 100 MHz): δ 143.1 (d, J_{CP} = 72.8 Hz, C_{ipso}), 134.2 (s, C═C), 131.2–131.1 (m, C_{meta}), 129.7–129.6 (m, C_{ortho}); ESI-LRMS (1%) *m/z* calcd for $[Lu(C_{26}H_{22}O_2P_2)_2(CF_3O_3S)_2(CF_3O_2SOH)(CH_3CN)]^{+}$: 1520.1, found 1520.1; CHN analysis for Lu(**1**)$_3$(OTf)$_3$(Et$_2$O)$_2$ calculated (found): C 52.00 (52.25), H 4.22 (3.77), N 0.00 (0.00).

2.4. Solution speciation analysis by NMR titration

A small shell vial was charged with $dppeO_2$ (5 mg, 0.012 mmol) and dissolved in 750 μL $CDCl_3$. This solution was transferred to an NMR tube and analyzed by ^{1}H and ^{31}P NMR spectroscopy. A stock solution of the

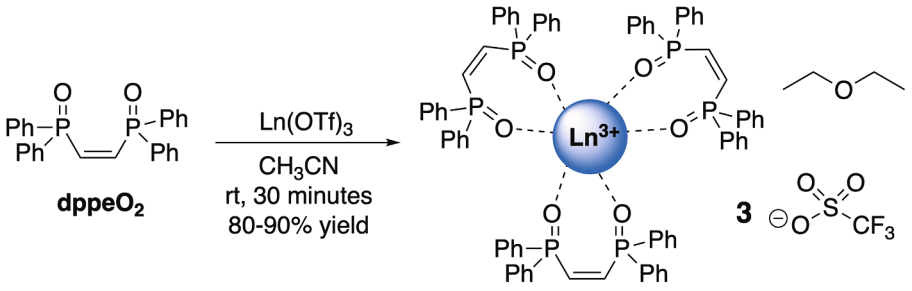

Scheme 1. Synthesis of $[Ln(dppeO_2)_3(OTf)_3(Et_2O)]$ complexes (Ln = La, Sm, Lu). In the complexes, the triflate groups are present as a mixture of inner sphere and outer sphere counteranions (rather than the pure outer sphere anions depicted here, *vide infra*) and a monoetherate is observed after purification.

$Ln(OTf)_3$ in acetonitrile was prepared (0.180 M for Ln = La and Sm; 0.079 M for Ln = Lu) and varying volumes of this solution were added to the NMR tube in order to prepare solutions with ligand–metal stoichiometries that ranged from 1:0 to 5:1. After each addition of $Ln(OTf)_3$, the solution was shaken and allowed to equilibrate for approximately five minutes before analysis by ^1H and ^{31}P NMR.

3. Results and discussion

3.1. Synthesis and initial characterization of complexes

The $dppeO_2$ ligand was prepared following literature procedures [13,28]. The metal–ligand complexes were prepared by stirring $dppeO_2$ with the $Ln(OTf)_3$ of choice (Ln = La, Sm, Lu) in a 1:3 ratio in acetonitrile (Scheme 1). This metal–ligand stoichiometry was chosen based on previous work from our group [13,29] and others [30–32] where ligands similar to $dppeO_2$ formed complexes with lanthanide and actinide metals with stoichiometries ranging from two to four ligands per metal. The complexes were purified by trituration with diethyl ether to give off-white powders in reasonable yields. These powders were characterized by ^1H, ^{13}C and ^{31}P NMR in both $CDCl_3$ and CD_3CN. The signals for the ligand were slightly broadened in the presence of each metal, although the expected splitting patterns were still interpretable. These spectra are shown in the Supplemental Information file, and the solution characterization of the complexes in described in more detail in a later section.

Characterization of the solid complexes with CHN analysis revealed the presence of one molecule of diethyl ether solvate per $[Ln(dppeO_2)_3(OTf)_3]$ complex. The complexes were also dissolved in acetonitrile and analyzed using low resolution electrospray ionization mass spectrometry (LR ESI-MS). Peaks for varying ratios of Ln^{3+} to ligand were observed, often with the loss of one or two triflate anions to obtain a charged species. In some cases, the charged complexes also contained acetonitrile, water or ether solvent molecules. The mass spectra for each complex are shown in the Supplemental Information file.

Characterization of the solid complexes using infrared (IR) spectroscopy revealed a shift in the peak corresponding to the P═O stretch to lower wavenumbers relative to the $dppeO_2$ ligand alone (Table 1). The $\Delta\nu$ for the P═O stretch ranges from 17 to 25 cm^{-1} and is indicative of a weakening of the P═O bond upon coordination to the Ln^{3+} metal center. The stretch for the C═C bond is not changed in upon complexation to the Ln^{3+} metal.

3.2. Analysis of the solid complexes with single crystal X-ray diffraction

Single crystals of each complex were grown by dissolving the solid complex in methanol or methylene chloride in the presence of diethyl ether vapor at 4 °C. As described above, each complex was prepared with a 1:3 ratio between $Ln(OTf)_3$ and ligand **1**. In the case of the Sm^{3+} and Lu^{3+} crystals, this stoichiometry was retained in the single crystals that were analyzed. For the La^{3+} complex, however, crystals of complexes with different metal–ligand stoichiometries (1:2 and 1:4) were isolated and characterized. This result is an indication that the complexes are fluxional in solution, and that the structures discussed in this section represent snapshots of the dynamic nature of these lanthanide-ligand complexes. Information about the crystallographic data for each structure is given in Table 2, while Table 3 lists relevant bond lengths and angles. Abbreviated drawings of each complex are given in the figures below, while complete drawings showing the thermal ellipsoids and atom labeling scheme can be found in the Supplementary Information file.

Table 1
Infrared absorption bands (cm^{-1}) of $dppeO_2$ and the $[Ln(dppeO_2)_3(OTf)_3]$ complexes.

Compound	ν(P═O)	ν(C═C)
$dppeO_2$	1172	1437
$La(dppeO_2)_3(OTf)_3$	1155	1438
$Sm(dppeO_2)_3(OTf)_3$	1147	1439
$Lu(dppeO_2)_3(OTf)_3$	1147	1438

1. $[La(dppeO_2)_4(OTf)_3]$. The first crystalline La^{3+}-$dppeO_2$ complex that was analyzed by X-Ray diffraction contained a La^{3+} metal center that is coordinated to four bidentate $dppeO_2$ ligands, in spite of the preparation of this complex with a 1:3 metal–ligand ratio (Fig. 1, left). All three triflate anions are located in the outer sphere of the coordination complex, and all three were disordered (along with one benzene ring of a ligand). Additional electron density corresponding to what, we propose, is a mixture of disordered acetone and methanol molecules were removed using the BYPASS command [26] as executed by Olex2 [33,34]. Details describing the location of the removed electron density, as well as how the disordered benzene ring and triflate anions were modeled are given in the Supplementary Information file.

Analysis of the geometry of this eight-coordinate La^{3+} complex with the program SHAPE [35,36] suggests that it resembles a distorted square antiprism. The four $dppeO_2$ ligands occupy two square planes that are nearly perpendicular to one another (Fig. 1, right). To quantitate the planarity of each pair of ligands we defined two planes in the complex where each plane contained the metal atom (La1) along with the four oxygen atoms of the coplanar $dppeO_2$ ligands (O1, O2, O1b, O2b and O1a, O2a, O1c, O2c). The root mean square (rms) deviation from an ideal plane for each pair of ligands was relatively small at 0.1628 and 0.1066, respectively, as calculated using MPLA command in ShelXL, with an angle between these planes of 89.169 (0.051)°.

2. $[La(dppeO_2)_2(OTf)_3(H_2O)_2]$. This La^{3+}-ligand complex crystallized with two crystallographically unique complexes in the asymmetric unit, both with identical features (Fig. 2, left). The La^{3+} center is surrounded by two bidentate $dppeO_2$ ligands, two triflate anions and two water molecules. The adventitious water molecules in this complex are likely from the solvents used in the crystallization experiments. The third triflate anion is held close to the inner coordination sphere of the metal through two hydrogen bonds with the La^{3+}-bound aqua ligands. The metal is eight-coordinate with a geometry of the inner-coordination sphere that most closely resembles a square antiprism as determined using the program SHAPE [35,36]. The two bidentate $dppeO_2$ ligands are again nearly coplanar with a slightly higher rms deviation of 0.2124 and 0.2267 from ideality as was seen with the $La(dppeO_2)_4(OTf)_3$ structure (Fig. 2, right). The coordinating oxygen atoms of the two aqua and two triflate ligands are also nearly coplanar with rms deviations of 0.2364 and 0.2386 from an ideal plane. The plane containing the triflate and aqua ligands is nearly perpendicular to that of the *cis*-$dppeO_2$ ligands with an angle between them of 85.240 (0.045) and 85.050 (0.044)° for each complex. Within this plane, the triflate ligands are oriented *trans* to one another with O-La-O angles of 146.15(9) and 146.97(9)°, while the aqua ligands are *cis* to one another with O-La-O angles of 76.81(9) and 77.93(10)°.

3. $[Sm(dppeO_2)_3(OTf)_3(Et_2O)]$. Single crystals of the $dppeO_2$ ligand complexed with Sm^{3+} have three ligands bound to the metal center, all in a bidentate manner (Fig. 3). The inner-coordination sphere of the metal is completed with one triflate anion that is bound to the metal through one oxygen atom. The two remaining triflate anions are present in the outer coordination sphere of the complex, along with a single molecule of diethyl ether. The outer sphere triflate anions along with two benzene rings of the ligands were disordered. Further details regarding the modeling of this disorder are provided in the Supplementary Information file. The Sm^{3+} metal is coordinated by seven oxygen atoms in this structure, and the arrangement of these atoms resembles a distorted capped trigonal prism as determined using the program SHAPE [35,36]. None of the three bidentate $dppeO_2$ ligands are coplanar, as seen with the 8-coordinate structures described above. Instead, the ligands occupy the six points of the trigonal prism with the

Table 2
Crystal data and structure refinement information for the $[Ln(dppeO_2)_n(OTf)_3]$ complexes.

Complex	$[La(dppeO_2)_4(OTf)_3]$	$[La(dppeO_2)_2(OTf)_3(H_2O)_2]$	$[Sm(dppeO_2)_3(OTf)_3(Et_2O)]$	$[Lu(dppeO_2)_3(OTf)_3(H_2O)_2]$
CCDC Number	2279913	2279915	2279919	2279921
Empirical formula	$C_{107}H_{88}F_9LaO_{17}P_8S_3$	$C_{55}H_{48}F_9LaO_{15}P_4S_3$	$C_{85}H_{75}F_9O_{16}P_6S_3Sm$	$C_{81}H_{70}F_9LuO_{17}P_6S_3$
Formula weight	2299.62	1478.90	1955.80	1943.34
Temperature/K	100(2)	173(2)	100.20(10)	100.0(3)
Crystal system	triclinic	monoclinic	monoclinic	monoclinic
Space group	*P*-1	$P2_1/n$	$P2_1/n$	*P2/c*
a/Å	14.2659(3)	18.5759(16)	15.83452(15)	28.9857(18)
b/Å	14.90161(16)	32.054(3)	30.0593(2)	15.0801(10)
c/Å	26.6190(2)	20.8055(18)	19.02153(14)	22.1416(11)
α/°	102.1643(9)	90	90	90
β/°	90.2598(12)	101.3042(10)	101.7365(8)	108.813(6)
γ/°	105.7130(14)	90	90	90
Volume/Å^3	5313.59(13)	12147.9(18)	8864.49(13)	9161.2(10)
Z	2	8	4	4
Reflections collected	85,781	232,425	92,509	68,941
Independent reflections	22,679 [R_{int} = 0.0635, R_{sigma} = 0.0520]	30,010 [R_{int} = 0.0893, R_{sigma} = 0.0643]	19,060 [R_{int} = 0.0771, R_{sigma} = 0.0497]	18,606 [R_{int} = 0.1654, R_{sigma} = 0.1459]
Final R indexes [I>=2σ (I)]	R_1 = 0.0595, wR_2 = 0.1829	R_1 = 0.0545, wR_2 = 0.1311	R_1 = 0.0910, wR_2 = 0.2434	R_1 = 0.1394, wR_2 = 0.2811
Final R indexes [all data]	R_1 = 0.0658, wR_2 = 0.1953	R_1 = 0.0889, wR_2 = 0.1552	R_1 = 0.0975, wR_2 = 0.2516	R_1 = 0.1851, wR_2 = 0.3005

Table 3
Selected bond lengths (Å) and angles (°) for the single crystal X-Ray diffraction structures of the $Ln(dppeO_2)_n(OTf)_3$ complexes. For complexes with multiple bonds and angles of the same type, a range is given.

	$[La(dppeO_2)_4(OTf)_3]$	$[La(dppeO_2)_2(OTf)_3(H_2O)_2]$	$[Sm(dppeO_2)_3(OTf)_3(Et_2O)]$	$[Lu(dppeO_2)_3(OTf)_3(H_2O)_2]$
P═O–Ln	2.409(3)–2.612(3)	2.435(3)–2.478(3)	2.304(5)–2.397(4)	2.461(7)–2.481(8)
H_2O–Ln	——	2.512(3)–2.560(3)	——	2.503(8)
TfO–Ln	——	2.515(3)–2.562(3)	2.460(4)	2.582(7)
(P)O–Ln–O(P)*	68.09 (9)–70.02 (9)	70.78(9)–71.94(9)	75.21(16)–76.9(2)	67.6(3)–71.6(2)

*these P═O groups belong to the same $dppeO_2$ ligand.

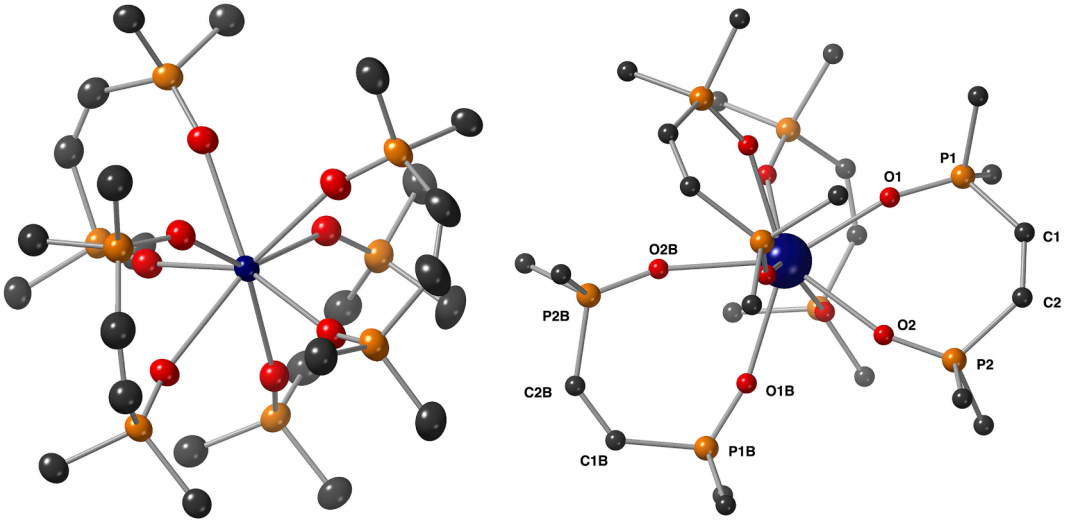

Fig. 1. Left: An abbreviated drawing of the $[La(dppeO_2)_4(OTf)_3]$ complex using standard CPK colors (La = dark blue) with the thermal ellipsoids drawn at the 50% probability level. Right: A drawing of the same complex using a ball and stick model showing the atom labeling scheme for selected atoms. All hydrogen atoms, the pendant phenyl rings, and the triflate anions have been omitted for clarity.

triflate anion occupying the capping position over the square faces.

The Sm^{3+}-bound triflate in this complex adopts two orientations (Fig. 4). The atom O1t is bonded to the metal and is located in a single position. The remainder of this triflate ligand is located over two orientations that are related by a ~60° rotation around the La-O1t bond. The relative occupancy of these two orientations was refined against a free variable and found to be 0.700(6):0.300(6). A possible reason for the presence of two orientations is that this triflate ligand is able to fill the space of two potential Sm^{3+} binding sites. While the second binding site is too small for another triflate ligand, it may have been able to be filled by a smaller solvent molecule (e.g. H_2O), had one been available. We propose this based on the structure obtained for the Lu^{3+} complex (*vide infra*), which has a smaller ionic radius than Sm^{3+} but accommodates eight coordinated oxygen atoms (rather than the seven oxygen atoms bonded by this Sm^{3+} atom).

4. $[Lu(dppeO_2)_3(OTf)_3(H_2O)_2]$. The structure of the [Lu

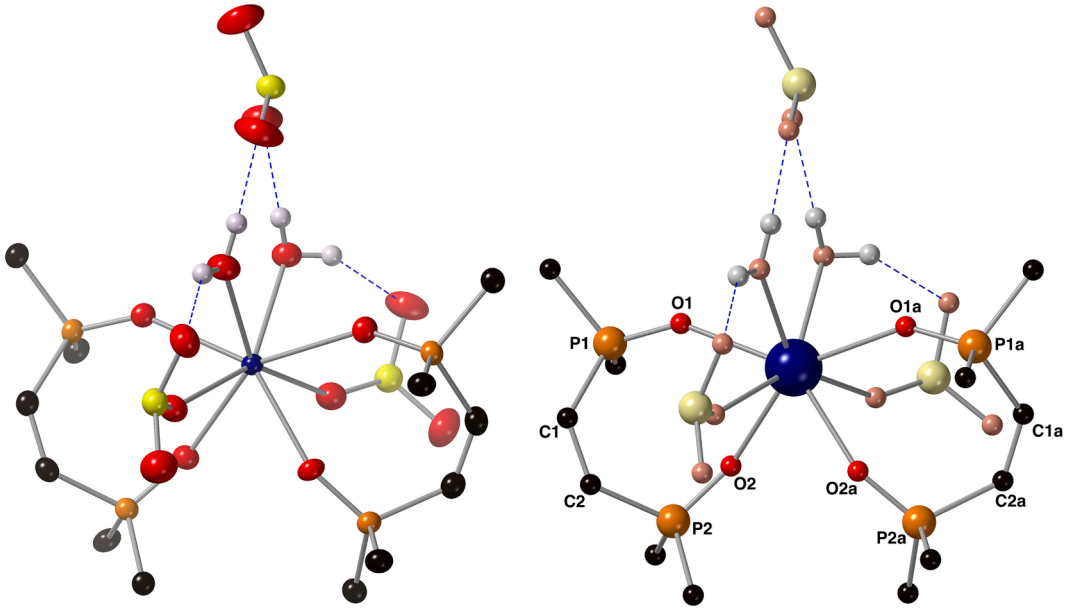

Fig. 2. Left: An abbreviated drawing of the crystal structure of the $[La(dppeO_2)_2(OTf)_3(H_2O)_2]$ complex using standard CPK colors (La = dark blue) with the thermal ellipsoids set at the 50% probability level. Only one complex of the asymmetric unit is shown, and hydrogen atoms not engaged in a hydrogen bond have been omitted for clarity. Hydrogen bonding interactions are drawn with blue, dashed lines. Right: A drawing of the same complex using a ball-and-stick model showing the inner coordination sphere of the metal and the partial atom naming scheme. All hydrogen atoms (except for those on the aqua ligands), the pendant phenyl rings and the $-CF_3$ groups of the triflate anions are not shown for clarity.

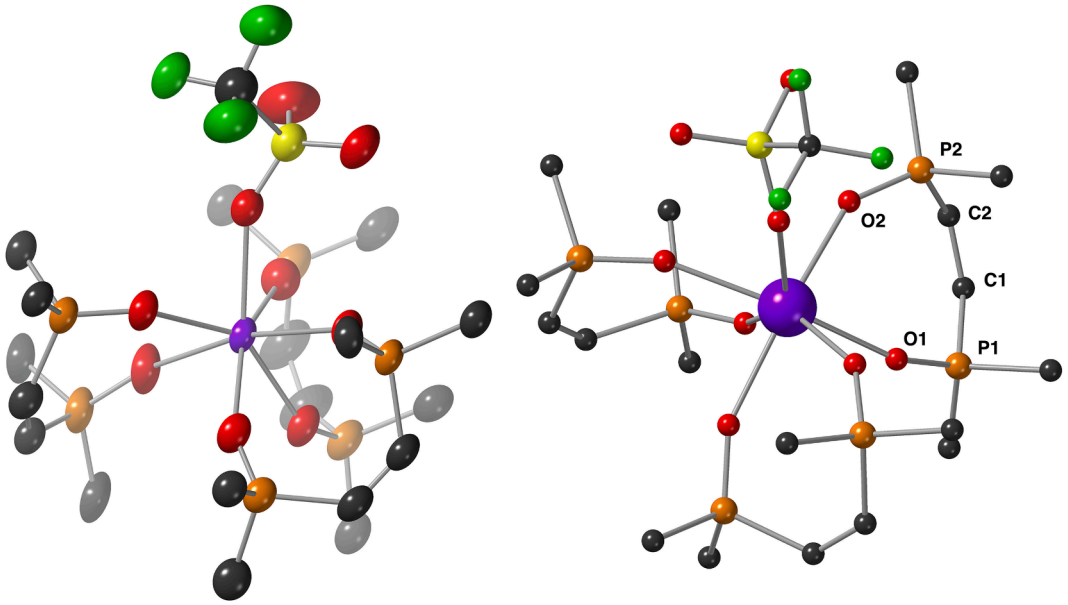

Fig. 3. Left: An abbreviated drawing of the $[Sm(dppeO_2)_3(OTf)_3]$ complex with the thermal ellipsoids drawn at the 50% probability level using standard CPK colors (Sm = purple). Right: A drawing of the same complex using a ball-and-stick model showing the atom labeling scheme of one ligand. In both drawings the outer sphere triflates, pendant phenyl rings, solvent diethyl ether and all hydrogen atoms have been omitted for clarity.

$(dppeO_2)_3(OTf)_3]$ complex is overall eight-coordinate, with three bidentate $dppeO_2$ molecules coordinated to the metal along with one inner sphere triflate ligand and one aqua ligand (Fig. 5, left). Of the four structures discussed here, this one has the lowest symmetry. The aqua ligand forms hydrogen bonds with a second-sphere water molecule and a partially occupied triflate anion that is not bonded to the metal (*vide infra*). When the geometry of the eight Lu^{3+}-bound oxygen atoms were analyzed using the program SHAPE [35,36], the geometry of the complex most closely resembles a triangular dodecahedron. The arrangement of ligands around the Lu^{3+} metal resembles the 8-coordinate complexes isolated with La^{3+} as the metal, with two perpendicular planes of ligands. One of these planes is occupied by two $dppeO_2$ ligands, while the other holds one ligand along with the triflate and water molecules.

This structure contained a significant number of disordered atoms that stem from the partial occupancy of a triflate anion in the second coordination sphere (Fig. 5). A partially occupied triflate anion is held via a hydrogen bond to a second-sphere water molecule and is found in a hydrophobic pocket created by the benzene rings of the ligands. When this triflate anion is present in this pocket, the benzene rings shift

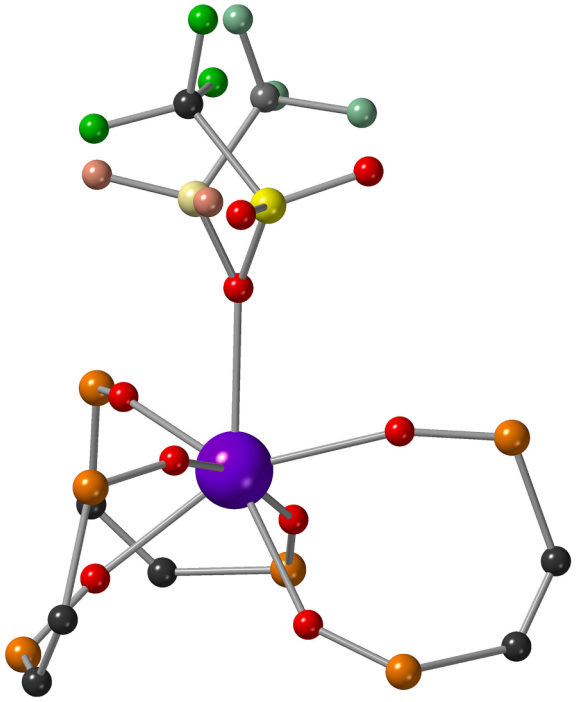

Fig. 4. An abbreviated drawing of the [Sm(dppeO$_2$)$_3$(OTf)$_3$(Et$_2$O)] complex showing the two orientations of the metal-bound triflate ligand using a ball-and-stick model.

slightly outward to accommodate the triflate, and this shifting reverberates through almost all the atoms of one dppeO$_2$ ligand. When the triflate anion is not present in the hydrophobic pocket it is found in the outer coordination sphere of the complex. In the absence of the triflate anion the benzene rings of the ligands shift toward one another in an attempt to fill the vacated space. Interestingly, the single water molecule found in the second coordination sphere is present 100% of the time and is held there through a hydrogen bond with the Lu^{3+} bound aqua ligand.

When looking at these four structures we see that the coordination number of the complexes does not decrease across the series as the size of the Ln^{3+} ion decreases. Each of the crystalline complexes analyzed in this work has a coordination number of eight, with the exception of the Sm^{3+} complex at seven. It is noted above, however, that the Sm^{3+} complex has an open coordination site that is filled through a disordered triflate ligand. What does change about these complexes, however, is the composition of the ligands in the inner coordination sphere. Only the largest ion of the series, La^{3+}, has been shown to be able to accommodate four dppeO$_2$ ligands. The complexes involving the smaller Sm^{3+} and Lu^{3+} ions only bond to three dppeO$_2$ ligands and fill the remaining coordination sites with the smaller triflate and aqua ligands.

3.3. Solution studies of complexes using ^{1}H and ^{31}P NMR

With the solid-state crystallography data in hand, we turned our efforts to investigating the structure of these [Ln(dppeO$_2$)$_n$(OTf)$_3$] complexes in solution. We were particularly interested to see how the identity of the Ln^{3+} metal affected the NMR spectra and if different complex stoichiometries could be observed in solution. To do this we carried out NMR titration experiments [37,38] for each Ln(OTf)$_3$-ligand complex where we added incremental amounts of Ln(OTf)$_3$ (dissolved in CD$_3$CN) to a solution of dppeO$_2$ in CDCl$_3$. The reason for the mixed-solvent system is that, ironically, the Ln(OTf)$_3$ is poorly soluble in CDCl$_3$ while dppeO$_2$ is poorly soluble in CD$_3$CN. The Ln^{3+}-ligand ratio was varied from 1:1 to 1:5 to move through the stoichiometric extremes of the coordination complexes. In a solution with a 1:1 Ln^{3+}-ligand ratio we propose, based on the NMR spectra, that every ligand present in solution is coordinated to a metal. What we are not able to determine, however, is if every metal is bonded to a dppeO$_2$ ligand. In contrast, when more than four equivalents of ligand are present we propose that there will be ligand in solution that is not bound in a bidentate manner to the inner coordination sphere of the metal. This hypothesis is based on the La(dppeO$_2$)$_4$(OTf)$_3$ crystal structure described above where the La^{3+} metal is completely saturated with four equivalents of ligand.

The results of the titration experiment with La(OTf)$_3$ are shown in Fig. 6. In the ^{1}H NMR spectrum of dppeO$_2$ alone, the signal for the vinylic hydrogen atoms is overlapped with the residual CHCl$_3$ solvent,

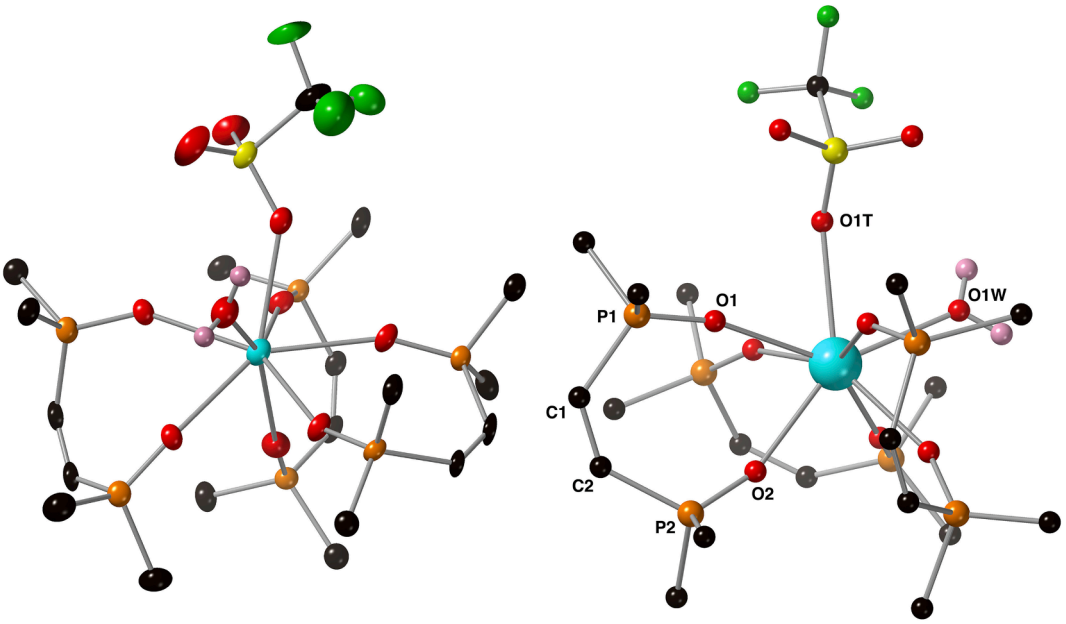

Fig. 5. Left: Abbreviated structure of the major component of the [Lu(dppeO$_2$)$_3$(OTf)$_3$(H$_2$O)$_2$] complex with the thermal ellipsoids drawn at the 50% probability level using standard CPK colors (Lu = light blue). The pendant phenyl rings, outer sphere water and triflate anions, and all hydrogen atoms other than those bonded to an oxygen atom have been omitted for clarity. Right: The same complex drawn using a ball-and-stick model with the atom labeling scheme for the aqua ligand, one oxygen atom of the inner sphere triflate and one dppeO$_2$ ligand.

and the signal for the *para*-hydrogen atom of the aromatic rings can be identified by integration. The ^{31}P NMR spectrum shows one sharp signal around 20 ppm for the two equivalent phosphorus atoms of the ligand. When the solution contains a 1:1 ratio of La^{3+} to $dppeO_2$ the signals for the aromatic hydrogen atoms shift slightly upfield and, unfortunately, the resonance for the vinylic hydrogen atoms broadens and can no longer be identified with any certainty. Based on the results of the other titration experiments described here (*vide infra*) we suspect that due to these hydrogen atoms' proximity to the chelating groups of the ligand this signal shifts downfield but remains obscured by the signal for $CHCl_3$. The ^{31}P NMR spectrum shows one sharp singlet that is shifted downfield 4.5 ppm relative to the signal for $dppeO_2$ alone. Both spectra contain one set of signals, indicating that Ln^{3+}-ligand exchange is at a rate that is fast on both the ^{1}H and ^{31}P NMR time scales.

As the equivalents of ligand are increased, the position of the signals for the aromatic hydrogen atoms in the ^{1}H NMR spectra shift slowly downfield and broaden significantly. We suspect that the signal for the vinylic hydrogen atoms continues to resonate near the $CHCl_3$ residual solvent signal (~7.8 ppm), but we are unable to assign this with any certainty. The signal in the ^{31}P NMR also broadens as the amount of ligand is increased, until at 4.5 equivalents of $dppeO_2$ one can observe two distinct resonances between 20 and 30 ppm. The signal broadness observed at the higher La^{3+}-ligand ratios is likely due to a slower rate of exchange in the presence of excess ligand, which becomes slow on the ^{31}P NMR time scale but remains intermediate on the ^{1}H NMR time scale.

The question then remains – why does the rate of ligand exchange decrease as the amount of ligand in solution is increased? To answer this question, we look back to the X-Ray crystal structures of the La^{3+}-$dppeO_2$ complex described above where complexes with both a 1:2 and 1:4 La^{3+}-ligand ratio were observed. Our hypothesis here is that as more equivalents of ligand are added to the inner-coordination sphere of the metal, the complex becomes more sterically burdened and on–off ligand exchange becomes more difficult. Also based on those crystal structures we propose that a La^{3+} metal cannot accommodate more than four bidentate $dppeO_2$ ligands in its inner coordination sphere. For the solutions in this titration experiment with more than four equivalents of ligand present, if truly "free" ligand were present in solution we would expect to see a sharp singlet at 21.1 ppm. These broad signals likely, then, correspond to La^{3+}-ligand complexes with differing geometries and stoichiometries. The easiest explanation for the different binding modes of $dppeO_2$ is that once the La^{3+} metal has become saturated with bidentate ligand, some ligands move to a monodentate mode of binding. Our group has published crystallographic evidence of this type of binding with $Th(NO_3)_4$ where a water molecule replaced one oxygen atom of a $dppeO_2$ ligand in the inner coordination sphere of the complex [13]. The Th^{4+}-bound water molecule was also engaged in a hydrogen bond with the displaced oxygen atom of the $dppeO_2$ ligand, making the ligand's binding mode pseudo-bidentate. We propose that a similar equilibrium exists in these solutions and that, in addition to on–off metal exchange, exchange between bidentate and pseudo-bidentate binding modes is possible.

The results of the titration experiment with $Sm(OTf)_3$ are similar in many ways to that with $La(OTf)_3$. In the ^{1}H NMR spectra the signals for the aromatic hydrogen atoms broaden in the presence of Sm^{3+}, and shift in a similar way to that observed for La^{3+}. While some of the line broadening observed in these spectra could be due to the paramagnetism of Sm^{3+}, we believe that some of the broadening is due to metal–ligand exchange processes. The most significant difference with the Sm^{3+} complexes is that the resonance for the vinylic hydrogen atoms is observable for Sm^{3+}-$dppeO_2$ ratios up to three equivalents of ligand, at which point the signal broadens into the baseline. This signal is shifted downfield relative to that of the free ligand, with a $\Delta\delta$ of ~0.77 for the

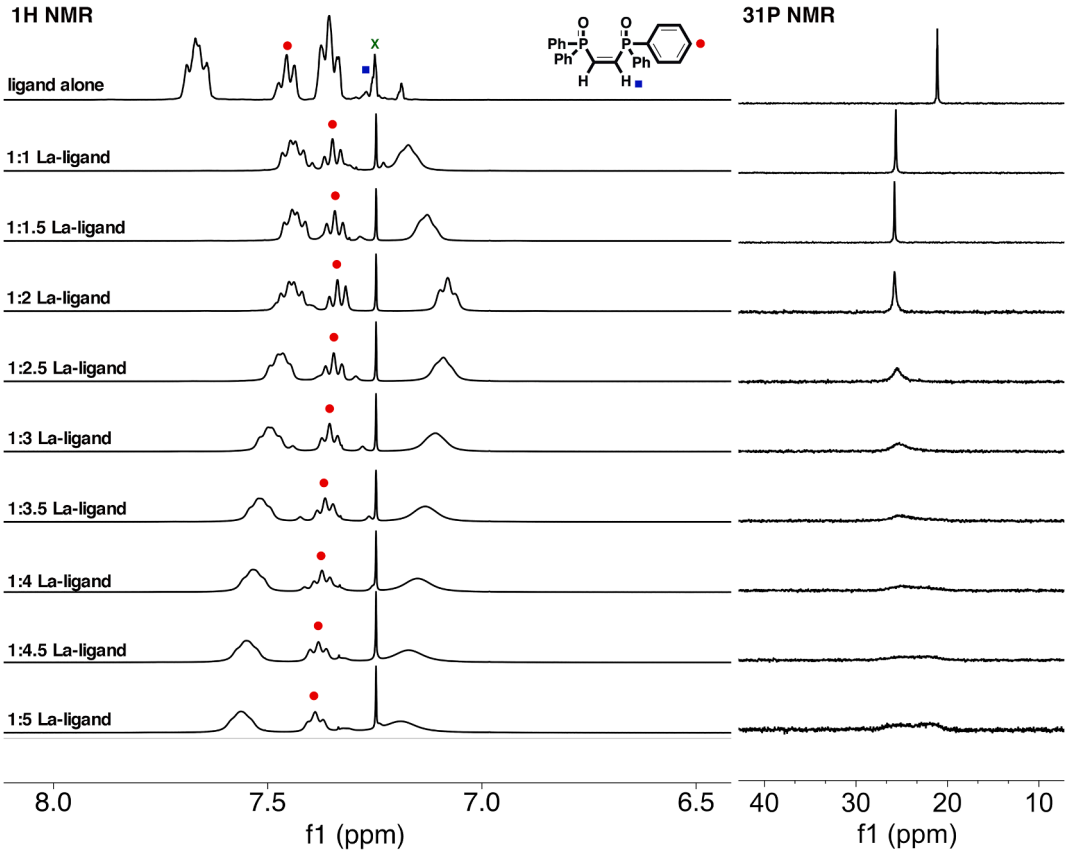

Fig. 6. ^{1}H and ^{31}P NMR spectra (^{1}H = 400 MHz, $CDCl_3$) of solutions containing varied ratios of $La(OTf)_3$ to $dppeO_2$. In the ^{1}H NMR spectra, signals are marked as: $dppeO_2$ vinylic hydrogen (blue circle), $dppeO_2$ phenyl ring *para* hydrogen (red square), residual $CHCl_3$ (green x).

1:1 complex (approximating a chemical shift of 7.25 for the vinylic hydrogen atoms of dppeO$_2$ alone). For all Sm^{3+}-dppeO$_2$ ratios one set of signals are observed, indicating fast or intermediate exchange on the ^{1}H NMR time scale.

The ^{31}P NMR spectra of the Sm^{3+} complexes are nearly identical to those obtained for the La^{3+} complexes (Fig. 7), with a series of downfield shifted, relatively sharp singlets for the 1:1 to 1:3 Sm^{3+}-dppeO$_2$ ratios. The signal of the phosphorus atoms in the 1:1 complex is shifted downfield 7.6 ppm relative to that of the free ligand, which is a slightly larger shift than when in the presence of La^{3+}. For the solutions with more than four equivalents of ligand, two broad signals are observed which we again assign to different coordination environments of the ligand.

Interestingly, the titration experiment with the Lu(OTf)$_3$ complexes revealed different behavior in solution (Fig. 8). The aromatic signals in the ^{1}H NMR spectra again broaden as the equivalents of ligand are increased, and the signal for the vinylic hydrogen atoms is only assignable for Lu^{3+}-dppeO$_2$ ratios of 1:2.5 to 1:4.5. The ^{31}P NMR spectra, however, are much more informative. At a 1:1 Lu^{3+}-dppeO$_2$ ratio, two signals are observed that are relatively sharp, overlap, and are shifted 8.5 ppm downfield from the resonance of dppeO$_2$ alone. This signal merges into one singlet (29.5 ppm) for the solution with a 1:1.5 Lu^{3+}-ligand ratio, with a small new resonance appearing slightly upfield (28.7 ppm). This upfield signal grows at the expense of the original resonance as the equivalents of ligand are increased, until it is the only signal present in the spectrum when a 1:3 Lu^{3+}-ligand ratio is present. We assign the signal at 29.5 ppm to a rapidly equilibrating mixture of complexes with 1:1 and 1:2 Lu^{3+}-dppeO$_2$ stoichiometries. We then assign the signal at 28.7 ppm to a ligand in a 1:3 Lu^{3+}-dppeO$_2$ complex and note that the presence of two signals in these spectra means that the ligands are undergoing exchange that is slow on the ^{31}P NMR time scale. We also find it interesting that for this point alone in the titration only one species is detectable by ^{31}P NMR.

The signal we attribute to the 1:3 Lu^{3+}-dppeO$_2$ complex persists as the equivalents of ligand are increased but broadens slightly throughout the remainder of the titration. A new signal appears in the presence of 3.5 equivalents of ligand, which could correspond to a small amount of a 1:4 Lu^{3+}-ligand complex. This signal also persists as the amount of ligand is increased and at four equivalents of ligand a third signal appears with the same chemical shift as that of free dppeO$_2$, albeit somewhat broadened.

We explain the slower exchange rate of the Lu^{3+}-complexes observed here again with a steric argument. In this case the ionic radius of Lu^{3+} is smaller than both La^{3+} and Sm^{3+}, which we propose makes ligand exchange more difficult to achieve. Another explanation could be that Lu^{3+} is more charge dense than the other metals, implying that the ligand-Lu^{3+} bond is stronger in these complexes and, hence, more difficult to disrupt.

To summarize the solution titration experiments, this data reinforces the concept that the [Ln(dppeO$_2$)$_n$(OTf)$_3$] complexes investigated in this work are a composition of dynamic species that interchange rapidly in solution. A number of factors affect the rate of this exchange including the identity of the Ln^{3+} metal, coordination ability of the solvent, complex concentration, anion, and steric bulk of the ligand. This paper investigated only the identity of the Ln^{3+} metal, but future studies that look into the effect of changing some of the other factors listed will be

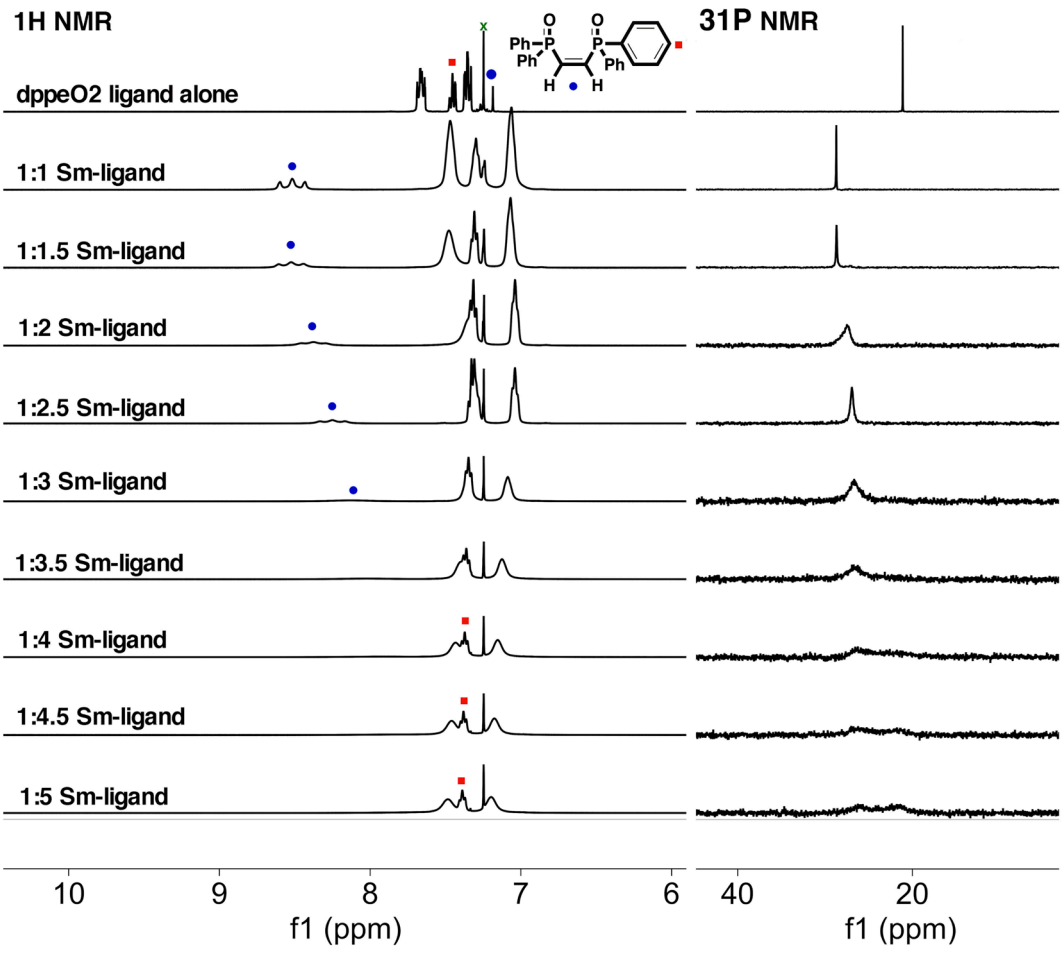

Fig. 7. ^{1}H and ^{31}P NMR spectra (^{1}H = 400 MHz, $CDCl_3$) of solutions containing varied ratios of Sm(OTf)$_3$ to dppeO$_2$. In the ^{1}H NMR spectra, signals are marked as: dppeO$_2$ vinylic hydrogen (blue circle), dppeO$_2$ phenyl ring *para*-hydrogen (red square), residual $CHCl_3$ (green x).

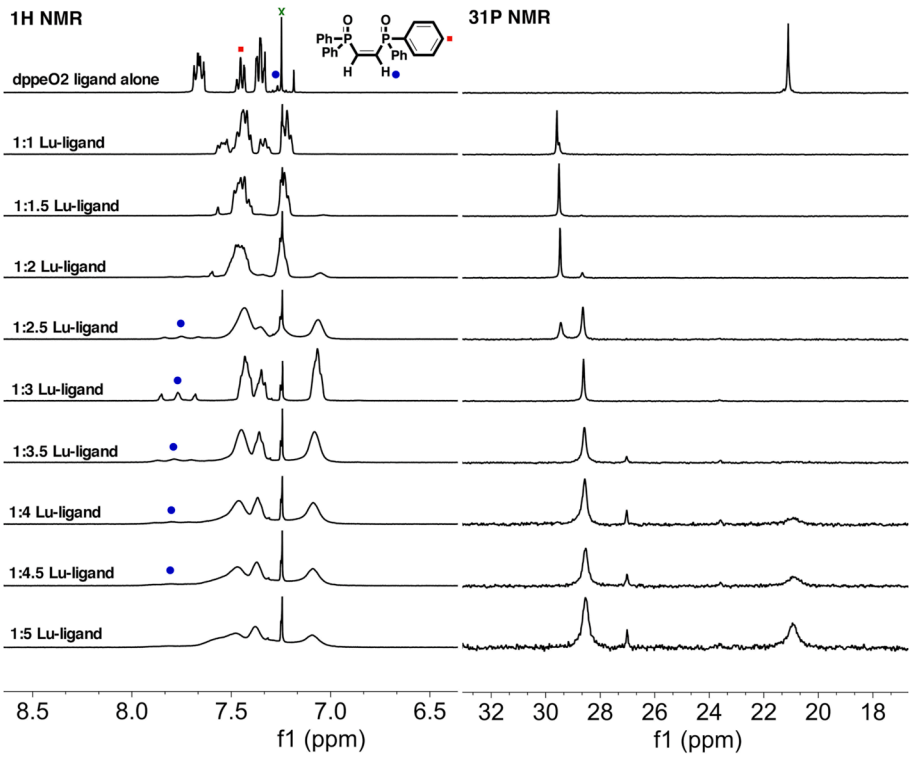

Fig. 8. ^{1}H and ^{31}P NMR spectra (^{1}H = 400 MHz, $CDCl_3$) of solutions containing varied ratios of $Lu(OTf)_3$ to $dppeO_2$. In the ^{1}H NMR spectra, signals are marked as: $dppeO_2$ vinylic hydrogen (blue circle), $dppeO_2$ phenyl ring *para* hydrogen (red square), residual $CHCl_3$ (green x).

forthcoming from our group.

4. Conclusions and outlook

This study investigated the binding properties of a relatively rigid, *bis*phosphine oxide ligand with three $Ln(OTf)_3$ salts (Ln = La, Sm, Lu) in both solution and the solid state. X-Ray crystallographic analysis showed that the ligand participated in only bidentate binding to these Ln^{3+} ions in the solid state to give seven- and eight-coordinate complexes. In solutions of $CDCl_3$ the Ln-ligand complexes give interpretable ^{1}H and ^{31}P NMR spectra, with some evidence that as the metal becomes sterically crowded with $dppeO_2$ ligand the exchange rate of the ligand slows.

Also learned from this study is some insight into the impact of the choice of Ln^{3+} metal on the NMR spectra of the resultant complexes. Based on this work it appears that complexes with La^{3+} will maintain the fine features of the signals, such a splitting patterns, but may give relatively small changes in the chemical shifts of the signals. For this system, complexes with Sm^{3+} showed some line broadening, but did have larger chemical shift changes relative to the signals for the free ligand. Lastly, one could consider studying complexation dynamics with Lu^{3+} since, in this work, these complexes had a slower exchange rate on the ^{31}P NMR time scale which allowed for the observation of multiple species in solution.

Future investigations into the solution dynamics of this system may include VT experiments and the exploration of a coordinating solvent (e.g. CH_3OH) on the exchange rate of the complexes. Our group is also interested in studying the phosphine sulfide and phosphine selenide derivatives [39,40] of this ligand and their ability to form complexes with actinide metals.

CRediT authorship contribution statement

Georgia G. Sands: Investigation, Data curation, Writing – original draft. **Grace Ertle:** Investigation. **Jimmy Mugemana:** Investigation. **Richard J. Staples:** Investigation. **John E. Bender:** Conceptualization, Methodology, Validation, Resources, Supervision, Project administration. **Shannon M. Biros:** Conceptualization, Methodology, Validation, Resources, Data curation, Writing – original draft, Writing – review & editing, Visualization, Supervision, Project administration, Funding acquisition.

Declaration of Competing Interest

The authors declare the following financial interests/personal relationships which may be considered as potential competing interests: Shannon Biros reports financial support was provided by National Science Foundation. Shannon Biros reports financial support was provided by Air Force Office of Scientific Research.

Data availability

Data will be made available on request.

Acknowledgements

We thank GVSU (CSCE, CUSE, Weldon Fund) and the Air Force Office of Scientific Research (AFOSR) Summer Faculty Fellowship Program (SFFP) for financial support, as well as the Barry M. Goldwater Foundation for a scholarship to G. Sands. We also thank Dr. S. Billinovich for support with all instrumentation at GVSU and Tim Bergeron (JEOL USA, Inc.) for help with NMR experiments.

Funding

We are grateful to the National Science Foundation for student (REU CHE-1062944 to G. Ertle and J. Mugemana; RUI CHE-2102576) and instrument (MRI CHE-1725699 - JEOL NMR; MRI CHE-1919817 - Advion HPLC-MS) support at GVSU, as well as at MSU (MRI CHE-1919565 – Rigaku XRD).

Appendix A. Supplementary data

The Electronic Supplementary Information file contains characterization data (^{1}H, ^{13}C, ^{31}P NMR, MS, IR, CHN) for all compounds described here. CCDC contains the supplementary crystallographic data for all structures reported here (2279913, 2279915, 2279919 and 2279921). These data can be obtained free of charge via http://www.ccdc.cam.ac.uk/conts/retrieving.html, or from the Cambridge Crystallographic Data Centre, 12 Union Road, Cambridge CB2 1EZ, UK; fax: (+44) 1223-336-033; or e-mail: deposit@ccdc.cam.ac.uk. Also contained in this document are figures showing the major component of each X-Ray crystal structure with the thermal displacement ellipsoids, atom numbering scheme and details regarding the modeling of any disordered electron density. Supplementary data to this article can be found online at https://doi.org/10.1016/j.poly.2023.116659.

References

[1] P. Jethva, M. Momin, T. Khan, A. Omri, Materials 15 (2022) 2374.
[2] C. Godfrin, A. Ferhat, R. Ballou, S. Klyatskaya, M. Ruben, W. Wernsdorfer, F. Balestro, Phys. Rev. Lett. 119 (2017), 187702.
[3] S.F. Ashley, B.A. Lindley, G.T. Parks, W.J. Nuttall, R. Gregg, K.W. Hesketh, U. Kannan, P.D. Krishnani, B. Singh, A. Thakur, M. Cowper, A. Talamo, Ann. Nucl. Energy 69 (2014) 314–330.
[4] H. Kolesnikov-Gauthier, N. Lemoine, E. Tresch-Bruneel, A. Olivier, A. Oudoux, N. Penel, Support. Care Cancer 26 (2007) 751–758.
[5] G.W. Kajjumba, E.J. Marti, Chemosphere 309 (2022), 136462.
[6] M. Keerthana, T. Pushpa Malini, R. Sangavi, J. Arockia Selvi, M. Arthanareeswari, Chem. Sel. 7 (2022), e202103610.
[7] M. Humayun, H. Ullah, M. Usman, A. Habibi-Yangjeh, A. Ali Tahir, C. Wang, W. Luo, J. Energy Chem. 66 (2022) 314–338.
[8] S. Banda, R. Pritchard, Orient. J. Chem. 24 (2008) 17–22.
[9] S. Dondi, M. Nardelli, C. Pelizzi, G. Pelizzi, G. Predieri, J. Chem. Soc., Dalton Trans. (1985) 487–491.
[10] P.G. Harrison, N.W. Sharpe, C. Pelizzi, G. Pelizzi, P. Tarasconi, J. Chem. Soc., Dalton Trans. (1983) 1687–1693.
[11] A. Wirth, O. Moers, A. Blaschette, P.G. Jones, Z. Anorg. Allg. Chem. 625 (1999) 982–988.
[12] Mothi, E. M.; Stoekli-Evans, H.; Panchanatheswaran, K., *Synth. React. Inorg., Met.-Org., Nano-Met. Chem.* **2016,** *46*, 1371-1375.
[13] P.T. Morse, R.J. Staples, S.M. Biros, Polyhedron - Special Issue on Undergraduate Research 114 (2016) 2–12.
[14] E. Makrlik, P. Vanura, Z. Spichal, J. Mol. Liq. 221 (2016) 574–578.
[15] V.P. Morgalyuk, N.P. Molochnikova, G.V. Myasoedova, I.G. Tananaev, Radiochemistry 48 (2006) 580–583.
[16] F. Arnaud-Neu, J.K. Browne, D. Byrne, D.J. Marrs, M.A. McKervey, P. O'Hagan, M. J. Schwing-Weill, A. Walker, Chem. Eur. J. 5 (1999) 175–186.
[17] A.M. Rozen, Z.I. Nikolotova, N.A. Kartasheva, Radiokhimiya 25 (1983) 609–613.
[18] M.K. Chmutova, N.E. Kochetkova, B.F. Myasoedov, J. Inorg. Nucl. Chem. 42 (1980) 897–903.
[19] K. Binnemans, P.T. Jones, B. Blanpain, T. Van Gerven, Y. Yang, A. Walton, M. Buchert, J. Clean. Prod. 51 (2013) 1–22.
[20] S.M. Jowitt, T.T. Werner, Z. Weng, G.M. Mudd, Curr. Opin. Green Sustain Chem. 13 (2018) 1–7.
[21] N. Tsoulfanidis, The Nuclear Fuel Cycle, American Nuclear Society, La Grange Park, 2013, p. 478.
[22] 1.61, C. v. COSMO v1.61 *Software for the CCD detector systems for determining data collection parameters*, Bruker Analytical X-ray Systems: Madison, WI, 2009.
[23] v2010.11-3, A. APEX2 v2010.11-3 *Software for the CCD detector system*, Bruker Analytical X-ray Systems: Madison, WI, 2010.
[24] 7.68A, S. v. SAINT v7.68A *Software for the Integration of CCD Detector System*, Bruker Analytical X-ray Systems: Madison, WI, 2010.
[25] R.H. Blessing, Acta Crystallogr. A51 (1995) 33–38.
[26] P. van der Sluis, A.L. Spek, Acta Crystallogr. A46 (1990) 194–201.
[27] Agilent. *CrysAlis Pro*, Yarnton, Oxforshire, England, 2014.
[28] A.M. Aguiar, D.J. Daigle, J. Am. Chem. Soc. 86 (1964) 2299–2300.
[29] E.G. Leach, J.R. Shady, A.C. Boyden, A. Emig, A.T. Henry, E.K. Connor, R. J. Staples, S. Schaertel, E.J. Werner, S.M. Biros, Dalton Trans. 46 (2017) 15458–15469.
[30] R. Babecki, A.W.G. Platt, J.C. Tebby, J. Fawcett, D.R. Russell, R. Little, Polyhedron 8 (1989) 1357–1360.
[31] R. Babecki, A.W.G. Platt, D.R. Russell, Inorg. Chim. Acta 171 (1990) 25–28.
[32] R. Babecki, A.W.G. Platt, J. Fawcett, J. Chem. Soc., Dalton Trans. (1992) 675–681.
[33] O.V. Dolomanov, L.J. Bourhis, R.J. Gildea, J.A.K. Howard, H. Puschmann, J. Appl. Crystallogr. 42 (2009) 339–341.
[34] L.J. Bourhis, O.V. Dolomanov, R.J. Gildea, J.A.K. Howard, H. Puschmann, Acta Crystallogr. A71 (2015) 59–75.
[35] D. Casanova, J. Cirera, M. Llunell, P. Alemany, D. Avnir, S. Alvarez, J. Am. Chem. Soc. 126 (2004) 1755–1763.
[36] Llunell, M.; Casanova, D.; Cirera, J.; Alemany, P.; Alvarez, S. *Shape, 2.1*, https://www.ee.ub.edu/, 2013.
[37] H.T. Sartain, S.N. McGraw, C.T. Lawrence, E.J. Werner, S.M. Biros, Inorg. Chim. Acta. 426 (2015) 126–135.
[38] T. Luster, H.J.V.d. Roovaart, K.J. Korman, G.G. Sands, K.M. Dunn, A. Spyker, R.J. Staples, S.M. Biros, J.E. Bender, *Dalton Trans.* 51 (2022) 9103-9115.
[39] S. Parkin, J. Cunningham, B. Rawls, J.E. Bender, R.J. Staples, S.M. Biros, Acta Crystallogr. E79 (2023) 246–253.
[40] B. Rawls, J. Cunningham, J.E. Bender, R.J. Staples, S.M. Biros, Acta Crystallogr. E79 (2023) 28–32.